ACS PHYSICAL CHEMISTRY Au
AN OPEN ACCESS JOURNAL OF THE AMERICAN CHEMICAL SOCIETY

pubs.acs.org/physchemau

Article

Binding Energy and Free Energy of Calcium Ion to Calmodulin EF-Hands with the Drude Polarizable Force Field

Qiaozhu Tan, Ye Ding, Zongyang Qiu, and Jing Huang*

Cite This: *ACS Phys. Chem Au* 2022, 2, 143−155

Read Online

ACCESS | Metrics & More | Article Recommendations | Supporting Information

ABSTRACT: Calcium ions are important messenger molecules in cells, which bind calcium-binding proteins to trigger many biochemical processes. We constructed four model systems, each containing one EF-hand loop of calmodulin with one calcium ion bound, and investigated the binding energy and free energy of Ca^{2+} by the quantum mechanics symmetry-adapted perturbation theory (SAPT) method and the molecular mechanics with the additive CHARMM36m (C36m) and the polarizable Drude force fields (FFs). Our results show that the explicit introduction of polarizability in the Drude not only yields considerably improved agreement with the binding energy calculated from the SAPT method but is also able to capture each component of the binding energies including electrostatic, induction, exchange, and dispersion terms. However, binding free energies computed with the Drude and the C36m FFs both deviated significantly from the experimental measurements. Detailed analysis indicated that one of main reasons might be that the strong interactions between Ca^{2+} and the side chain nitrogen of Asn/Gln in the Drude FF caused the distorted coordination geometries of calcium. Our work illustrated the importance of polarization in modeling ion−protein interactions and the difficulty in generating accurate and balanced FF models to represent the polarization effects.

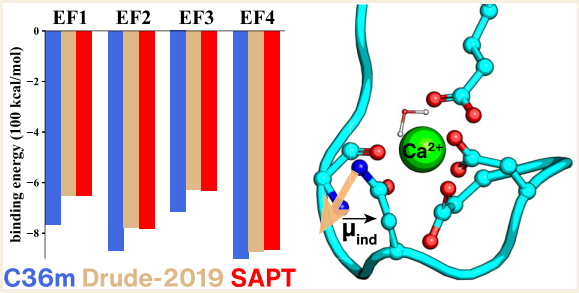

KEYWORDS: *Calcium ion, Calmodulin, CHARMM36m, Drude force field, binding free energy, polarization, ion-protein interaction*

INTRODUCTION

Calcium ions are key signaling molecules in living organisms and play crucial roles in muscle contraction, neuronal excitability, cell migration, and cell growth.[1] Most of these processes start with the binding of calcium ions with a calcium-binding or calcium-sensing protein, such as calmodulin (CaM).[2−6] The calcium-binding motif in CaM is a helix−loop−helix structure named EF-hand comprising 12 residues.[7] Each EF-hand can accommodate 1 calcium ion (Ca^{2+}) which coordinates with 7 oxygen atoms from the side chains of residues 1, 3, 5, and 12, the backbone of residue 7, and 1 water molecule as shown in Figure 1. Without calcium ions, the helices in the EF-hands are arranged in an antiparallel manner and the central linker in the CaM is disordered. The binding of calcium ions causes the conformation transition of EF-hand loops and thus induces large conformational change of CaM, so that its hydrophobic sites are exposed to recognize and activate target proteins,[7,8] which further initiates a variety of cellular processes that are key to maintaining life activities.

Calmodulin has been studied extensively through experimental and computational methods,[9−16] focusing on ion binding affinity and selectivity as well as the relationship between ion binding and protein functions. Yang et al. grafted each EF-hand loop of CaM into domain 1 of the CD2 protein to obtain the individual calcium affinity of four EF-hands, and found out their affinities were in the order I > III ≈ II > IV.[12] Lepvsik and Field performed quantum mechanics (QM) calculations and molecular dynamics (MD) simulations to obtain the binding energies between calcium ion and EF-hand loops of CaM.[13] Their results showed that the order of Ca^{2+}-binding affinity to CaM's EF-hand loops is I > III > IV > II, partially consistent with Yang's results. Xiao[14] used constrained dynamics with the AMBER PARM96 force field (FF) to calculate the binding free energies of calcium ions to the EF-hands. While the binding free energy of calcium ion to the EF1 was −5.4 kcal/mol that was in agreement with the experimental value, those of EF2 and EF4 were computed to be positive which deviated qualitatively from experimental results. These deviations were often attributed to the difficulty of additive FFs in describing the polarization effects of calcium ions.

It is challenging to develop accurate FF models for the calcium ion because of its strong polarization and charge-transfer effects, which can dramatically influence its solvation and interactions with biomolecules. Enormous efforts have

Received: October 27, 2021
Revised: December 9, 2021
Accepted: December 9, 2021
Published: December 28, 2021

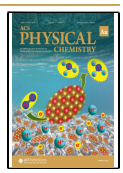

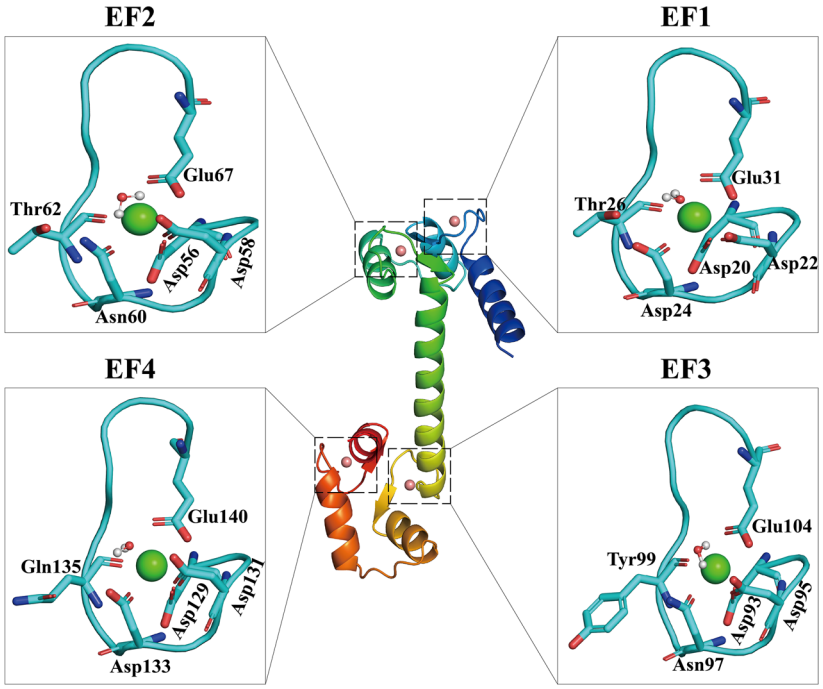

Figure 1. Structure of Calmodulin and its four EF-hand loops (PDB id: 1CLL).

been made in developing molecular mechanism (MM) models for Ca^{2+}, including charge-scaling schemes,[15,17] 12-6-4 Lennard-Jones-type nonbonded models proposed by Li et al.,[18−20] and multisite dummy atom models from Saxena's[21] and Song's groups.[22] The charge-scaling model is a convenient method to include electronic polarization effects for ions in aqueous and protein environments.[23,24] Kohagen and co-workers proposed to scale the charge of Ca^{2+} by 0.75 (from +2 to +1.5) to account for its polarization effects in a mean-field, average manner.[15,17] To keep the neutrality of the whole system, one has to scale the partial atomic charges on other atoms and two different schemes (ECCR and ECCR-P) were proposed depending on which atoms are scaled together with the calcium ions.

Another strategy is to explicitly model the polarization effects of calcium ions in the framework of polarizable force fields such as the AMOEBA and the Drude FF. Both polarizable FFs have been developed for water, ions, and a wide range of biomacromolecules such as proteins, nucleic acids, and lipids.[25−34] The AMOEBA FF utilizes a point induced dipole model to represent the polarization effects and higher-order moments up to quadrupole to treat electrostatic interactions accurately. The Drude FF adopts the classical Drude oscillator model which attaches an auxiliary Drude particle carrying a charge to the non-hydrogen atom with a harmonic spring, and the displacement of the Drude particle relative to its parent atom represents the influence of the external electric field. To facilitate the ability of the Drude FF to model nonbonded interactions, lone pair are included, which mimic the use of multipoles in AMOEBA. Recently, we demonstrated the equivalency of the point induced dipole model and the classical Drude oscillator model by mapping the Drude FF into an AMOEBA-like multipole and induced dipole model named MPID.[35]

Ren and co-workers used MD simulations with AMOEBA FF to study the selectivity and binding free energies for Ca^{2+} and Mg^{2+} to the EF-hand loops of calcium/magnesium-binding proteins including parvalbumin, calbindin D9k, a carboxylate cluster Mg-binding protein CheY, the C2 domain of dysferlin, and the integrin I domain.[36,37] Their calculations reproduced the relative binding free energies between Ca^{2+} and Mg^{2+} in different types of binding pockets defined by the number of carboxyl groups in the first/second shell of Ca^{2+}/Mg^{2+}. More importantly, they demonstrated that the selectivity of Ca^{2+} over Mg^{2+} due to the many-body interactions can be captured by the polarizable AMOEBA FF. In terms of the Drude model, Li et al. optimized the Drude FF parameters to accurately reproduce the interactions between ions (K^+, Na^+, Ca^{2+}, and Cl^-) and coordinating residues in 30 representative metalloprotein systems.[38] By targeting ab initio calculation (ion−protein coordination geometries and interaction energies) and experimental thermodynamical data (solvation free energies of ions), they obtained the pair-specific nonbonded LJ (NBFIX term in CHARMM) and through-space Thole screening (NBTHOLE term in CHARMM) parameters between ions and coordinating atoms of amino acids. This parameter set can be used together with the Drude-2013[30] or the Drude-2019[39] protein FF, and was shown to achieve good agreement in the binding energies between calcium ion and 10 Ca^{2+}-binding proteins with QM calculations at the B3LYP/CEP-121 level.[38] However, this study focused on chelated ions in binding sites, which might overestimate the binding affinity of ions with individual protein functional groups. Recently, Amin et al. have assessed the accuracy of Drude FFs in reproducing the interaction energy of Ca^{2+}-dipeptide against a comprehensive QM data set and proposed revised parameter sets to address the potential overpolarization of Asp and Glu side chains.[40] To our knowledge, there is no study performing binding free energy calculations of calcium ions to peptides or proteins with the Drude FF.

In this work, we investigated the binding energy and free energy of the calcium ion to CaM EF-hand loops with the most recent Drude-2019 polarizable FF and a fixed-charge additive protein FF, CHARMM36m (C36m).[41] Through

https://doi.org/10.1021/acsphyschemau.1c00039
ACS Phys. Chem Au 2022, 2, 143−155

comparison of interaction energies and energy components with the Symmetry-Adapted Perturbation Theory (SAPT) calculations, we demonstrated the advantage of explicit inclusion of polarization into FF models in describing ion−protein interactions. We also performed alchemical free energy perturbation (FEP) calculations with λ-state Hamiltonian replica exchange simulations to compute binding free energies of Ca^{2+} to the EF-hand loops, and showed that both Drude-2019 and C36m overestimated the binding of calcium ions to CaM EF-hands. We performed careful analyses on the ion coordination numbers and dipole moments during simulations. Our results highlight the necessity and difficulties to reparametrize the interaction between calcium ions and both Asn/Gln and Asp/Glu residues in the Drude FF.

The manuscript is organized as follows: Details of interaction energy calculations, energy decomposition analysis, MD simulations, FEP calculations, and trajectory analysis will be provided in the Methods section. In the Results section, the comparison of binding energies between Ca^{2+} and EF-hands will be presented first, followed by binding free energy results from FEP calculations. Detailed analyses of MD trajectories will then be presented. The manuscript will end with a short discussion and conclusion.

METHODS

Structure Preparation

The initial geometries were extracted from the crystal structure of CaM solved at 1.7 Å resolution (PDB id: 1CLL),[42] and their structures are shown in Figure 1. The four EF-hand loops marked as EF1, EF2, EF3, and EF4 comprise residue numbers 20−31, 56−67, 93−104, and 129−140, respectively. All four EF-hand loops were extracted with the calcium ion and a coordinating water molecule from the structure of CaM according to the residue numbers. Their sequences, coordinating positions, and total charges were summarized in Table S1. The N-terminus of EF-hand loops was the amino group (NH_2), while the C-terminus was the carboxyl group (COOH) in QM calculations. The four complexes contain 177, 163, 167, and 174 atoms, respectively, in QM calculations. In MD simulations, the EF-hand loops were capped with the acetylated group as the N-terminus and the *N*-methylamide group for the C-terminus.

The four EF-hand complex structures were optimized with the density functional theory (DFT) using the B3LYP functional.[43−45] The 6-311G(d,p) basis set was used for the C, H, O, N, and Ca atoms. The optimized geometries were validated by performing vibrational frequencies calculations, and used for subsequent interaction energy calculations and energy decomposition analysis. Geometry optimization and vibrational analysis were done using Gaussian 16.[46]

Energy Decomposition Analysis

The prediction of noncovalent interaction energies was carried out for Ca^{2+}/EF1, Ca^{2+}/EF2, Ca^{2+}/EF3, and Ca^{2+}/EF4 using the SAPT0 method with def2-TZVPD basis sets. The geometries used for SAPT calculations were the DFT-optimized structures. The interaction energies were decomposed into electrostatic, induction, exchange, and dispersion components. As a comparison, we also computed the binding energies of Ca^{2+} to the EF-hands at the B3LYP-D3/def2-TZVPD level. The binding energy between Ca^{2+} and EF-hands in the gas phase was defined by the following formula:

$$E_{bind} = E_{AB} - (E_A + E_B) \quad (1)$$

where E_{AB} is the energy of the complexes, E_A is the energy of the EF-hand loops plus the water molecule, and E_B is the energy of the calcium ion. Basis set superposition errors (BSSEs) were considered by the counterpoise procedure method.[47] The B3LYP-D3 calculations were carried out by Gaussian 16,[46] while the SAPT calculations were carried out using PSI4.[48]

The interaction energies and their energy components were also computed at the MM level using the DFT-optimized structures of calcium/EF-hand loops with the additive C36m and the polarizable Drude FFs, respectively. At the MM level, the interaction energies arise from the nonbonded energy terms in force fields, including the van der Waals (VdW) and electrostatic terms. The VdW term is formulated by a 12-6 Lennard-Jones potential in the CHARMM FFs and can be split into the C12 and C6 components that are considered to correspond to the repulsion and dispersion interactions in SAPT. While there is no induction term in the additive C36m FF, the electrostatic and induction terms are well-defined and can be separated in the Drude FF.

To perform energetic calculations with the Drude FF, the positions of the Drude particles need to be relaxed via energy minimizations with all the non-Drude particles fixed. Starting from the DFT-optimized complex geometry, the calcium ion (B) was removed and the Drude particles of the EF-hand loops plus the water molecule (A) were relaxed in the environment of A only, and the total electrostatic energy was labeled as $E_{A-mini-A}$. Similarly, the electrostatic energy of part B with Drude particles optimized in the environment of B was computed as $E_{B-mini-B}$. In this particular case, $E_{B-mini-B} = 0$ as part B is a single ion. Then, part B was added back with the coordinates of Drude particles kept, and the electrostatic energy of the complex was labeled as $E_{AB-non-mini}$. Finally, all Drude particles in the system were relaxed in the environment of the complex, and the total electrostatic energy was labeled as $E_{AB-mini-AB}$. From these, the electrostatic (E_{ele}) and induction (E_{ind}) components of the interactions between A and B can be obtained from these four components:

$$E_{ele} = E_{AB\text{-}non\text{-}mini} - E_{A\text{-}mini\text{-}A} - E_{B\text{-}mini\text{-}B}$$
$$E_{ind} = E_{AB\text{-}mini\text{-}AB} - E_{AB\text{-}non\text{-}mini} \quad (2)$$

We note that the harmonic bond energy between the Drude particle and its parent atom belongs to the electrostatic energy; however, it is classified as bonded energy in the current CHARMM code. Thus, the total energies obtained from CHARMM were directly used to calculate the E_{ele}.

MD Simulations

MD simulations of the four EF-hand complexes were performed with explicit solvent molecules. Complexes were solvated with 0.15 M KCl in 48 Å × 48 Å × 48 Å, 52 Å × 52 Å × 52 Å, 48 Å × 48 Å × 48 Å, and 51 Å × 51 Å × 51 Å cubic water boxes, respectively. The parameters for the amino acids and ions were taken from the C36m or the Drude-2019 force field. Correspondingly, water molecules were described by the TIP3P[49] or the SWM4-NDP model.[50] As periodic boundary condition (PBC) was applied, the electrostatic interactions were treated with Particle Mesh Ewald (PME)[51] with the splitting parameter $\kappa = 0.34$ and LJ interactions were truncated at 12 Å with a smooth switching off between 10 and 12 Å. The PME error tolerance parameter δ was set to 1.0^{-4}. The integration time step was 2 fs for the additive C36m FF and 1 fs for the polarizable Drude FF. Hydrogen-involved covalent bonds were constrained by the SHAKE algorithm.[52]

The systems were first equilibrated for 50 ps in canonical (NVT) ensemble at 310 K with the C36m FF. The final snapshots from equilibrated trajectories were extracted and used as the initial structure for 200 ns NPT simulations at 310 K and 1 atm with the C36m and the Drude-2019 FFs, respectively. Andersen thermostat[53] was used for C36m simulations, while the dual Langevin thermostats method[54] was used for Drude simulations with friction coefficients of 5 ps^{-1} for non-Drude atoms and 20 ps^{-1} for Drude particles. Drude hardwall constraint[33] was applied to avoid the separation between Drude particles and their parent atoms larger than 0.25 Å. Monte Carlo barostat was used to maintain the pressure.[55] The system setup and equilibrations were carried out in CHARMM[56,57] and 200 ns production runs were performed with OpenMM.[58]

https://doi.org/10.1021/acsphyschemau.1c00039
ACS Phys. Chem Au 2022, 2, 143−155

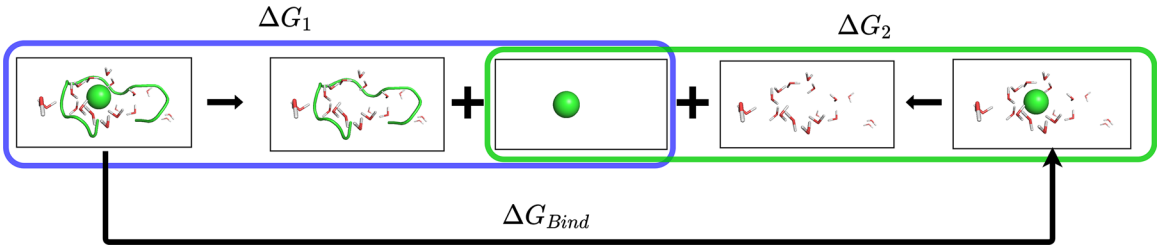

Figure 2. Binding free energy calculation protocol of calcium ion with EF-hand protein. ΔG_1 is the free energy difference when we remove calcium ion from EF-hand proteins and waters. ΔG_2 is the free energy difference when we remove calcium ion from bulk waters.

Table 1. Interaction Energies and Energy Components for the Binding of the Calcium Ion with Four EF-Hand Loops[a]

		EF1	EF2	EF3	EF4
electrostatic	C36m	−773.48	−872.79	−722.97	−976.74
	Drude-2019	−551.94	−675.96	−524.68	−778.71
	SAPT0	−544.45	−671.53	−526.15	−763.50
induction	C36m	0	0	0	0
	Drude-2019	−142.11	−134.02	−134.98	−137.18
	SAPT0	−167.39	−162.17	−164.87	−162.90
exchange	C36m	16.77	14.80	16.09	17.08
	Drude-2019	60.26	48.67	47.59	59.02
	SAPT0	75.29	65.36	71.87	73.88
dispersion	C36m	−9.57	−8.90	−9.35	−8.78
	Drude-2019	−17.26	−15.24	−16.32	−16.44
	SAPT0	−14.51	−13.44	−14.06	−13.38
total interaction	C36m	−766.27	−866.89	−716.23	−968.44
	Drude-2019	−651.05	−776.54	−628.39	−873.30
	SAPT0	−651.06	−781.79	−633.21	−865.89
	B3LYP-D3	−644.27	−777.61	−604.17	−859.21

[a]Units are kcal/mol.

Free Energy Calculations

The binding free energies of the calcium ion with EF-hand loops were calculated with the additive C36m and the polarizable Drude FFs, respectively. Each calculation consisted of two alchemical transformations. One was to gradually turn off interactions between the calcium ion with the EF-hand and solvent molecules as schemed in Figure 2 (blue box). The free energy change associated with this alchemical transformation was recorded as ΔG_1. The other one was designed to alchemically remove a calcium ion from the bulk water environment as shown in the green box in Figure 2. The difference of free energy was computed as ΔG_2, which was also known as the intrinsic hydration free energy of Ca^{2+}. With these two alchemical processes, the binding free energies ΔG_{Bind} of calcium ion with EF-hand loops can be computed as

$$\Delta G_{Bind} = \Delta G_1 - \Delta G_2 \quad (3)$$

To obtain the hydration free energy of Ca^{2+} that can be directly compared with experimental measurements, two corrections should be included as

$$\Delta G_{HFE} = \Delta G_2 + zF\phi - k_B T \ln(1/V_m) \quad (4)$$

where z is the ionic charge, F is the Faraday constant, and ϕ is the electrostatic Galvani potential at the liquid−vacuum interface. ϕ equals −545 mV and −500 mV for the SWM4-NDP and the TIP3P water models, respectively.[50,59,60] While the first correction term ($zF\phi$) accounts for the phase potential arising from an ion crossing the physical air/water interface, the second correction term ($-k_B T \ln(1/V_m)$) accounts for the entropic contribution of an ion going from an ideal gas to an idealized bulk solution at 1 M concentration.[59] V_m is the molar volume of an ideal gas, which equals 25.439 L/mol at 310 K and 1 atm.

Five independent systems were required for the alchemical free energy calculations, Ca^{2+}/EF1, Ca^{2+}/EF2, Ca^{2+}/EF3, Ca^{2+}/EF4, and Ca^{2+} in bulk water. The alchemical transformation of these systems was performed by the λ-state Hamiltonian replica exchange MD (H-REMD) simulation method[61] implemented in CHARMM. Thirty λ states were interpolated along the whole alchemical process to gradually turn off the nonbonded interaction between Ca^{2+} and EF-hand/water or bulk water. Electrostatic interactions were first turned off through 22 λ states, i.e., λ = 1.00, 0.95, 0.90, 0.85, 0.80, 0.75, 0.70, 0.65, 0.60, 0.60, 0.55, 0.50, 0.47, 0.43, 0.39, 0.35, 0.31, 0.26, 0.22, 0.18, 0.14, 0.10, 0.06, and 0.00. Then, LJ interactions were turned off in 8 states with λ = 1.00, 0.95, 0.77, 0.59, 0.41, 0.23, 0.05, and 0.00. The final conformations of 200 ns NPT trajectories generated by MD simulations described above were used as the initial structures for H-REMD simulations. All systems were propagated under velocity verlet integrator with 1 fs time step. NVT ensemble was realized with Nosé-Hoover algorithm[62,63] to keep the temperature at 310 K. For C36m simulations, the mass of the thermal piston of Nosé-Hoover was set to 500 kcal·ps^2/mol. For Drude simulations, the characteristic response time of Nosé-Hoover was set to be 0.1/0.005 ps for non-Drude/Drude particles. Exchanges were attempted between neighboring λ states every 1 ps and frames were saved every 1 ps. Free energy differences ΔG_1 and ΔG_2 were computed with the multistate Bennett acceptance ratio (MBAR) method[64] using Pymbar.[65]

RESULTS

Comparison of Binding Energies and Energy Components

We compared the binding energies of Ca^{2+} with EF-hand loops obtained by different QM and MM methods in Table 1. The total interaction energies computed by SAPT at the SAPT0/def2-TZVPD level were −651.06, −781.79, −633.21, and −865.89 kcal/mol for the four EF-hand complexes, respectively. Interaction energy calculations at the B3LYP-D3/def2-TZVPD level using eq 1 gave similar results, with slightly less

https://doi.org/10.1021/acsphyschemau.1c00039
ACS Phys. Chem Au 2022, 2, 143−155

negative values of −644.27, −777.61, −604.17, and −859.21 kcal/mol. We note that the interaction energies were systematically less favorable compared to the gas-phase QM calculations carried out by Lepšík and Field at the BP86/def2-SVP level that gave −709.3, −825.0, −662.5, and −890.7 kcal/mol.[13] The discrepancy was originated in the different number of water molecules included in the QM calculations. We only included one coordinating water molecule, while Lepšík and Field included the structural waters in the second coordinating shell as well. Nevertheless, both QM calculations in gas phase consistently predicted that calcium ion's binding stability in complexes was most favorable in the EF4 loop, and decreased in the order of EF2, EF1, and EF3.

As illustrated in Table 1 and Figure 3, binding energies from the Drude-2019 model were in good agreement with the SAPT

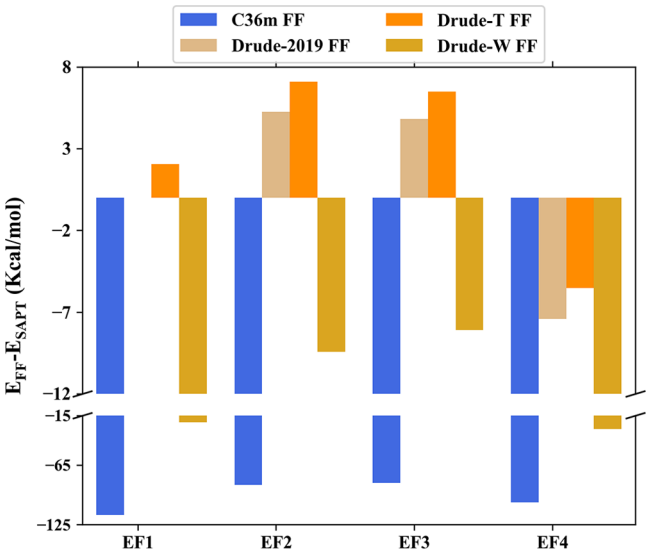

Figure 3. Binding energies calculated using FF models (C36m, Drude-2019, Drude-T, and Drude-W) relative to the SAPT values for the calcium ion with the four EF-hand loops (kcal/mol).

results. The differences in the binding energy were 0.01, 5.25, 4.82, and −7.41 kcal/mol for the four EF-hand complexes, respectively. The mean absolute error (MAE) equals 4.37 kcal/mol. In contrast, the C36m FF model has a significant overestimation of the interaction between Ca^{2+} and EF-loops. The binding energies were overestimated by −83 to −115 kcal/mol compared to SAPT results, with an MAE of 96.47 kcal/mol.

We performed energy decomposition analysis to further characterize the binding interaction between the calcium ion and EF-hand loops. The interaction energies were separated into electrostatic, induction, exchange, and dispersion terms. Based on SAPT calculations, electrostatics was the dominant component in the interaction energies, contributing −544.45 (83.62%), −671.53 (85.89%), −526.15 (83.09%), and −763.50 (88.17%) kcal/mol for EF1 to EF4 loops, respectively. Interestingly, although the amino acids in the four EF-hand loops are different, the induction energies are almost similar (Table 1). The exchange term contributes positive interaction energies from 65.36 to 75.29 kcal/mol, while dispersion makes Ca^{2+} attractive with EF-hand loops by about −14 kcal/mol.

The Drude-2019 FF not only reproduced the total binding interaction energy between the calcium ion and EF-hand loops, but was also able to capture each component as shown in Table 1. The permanent electrostatic energies from Drude-2019 calculations were in good agreement with the SAPT results, with the difference being −7.49, −4.43, 1.47, −15.21 kcal/mol, respectively (Figure 4). The induction components

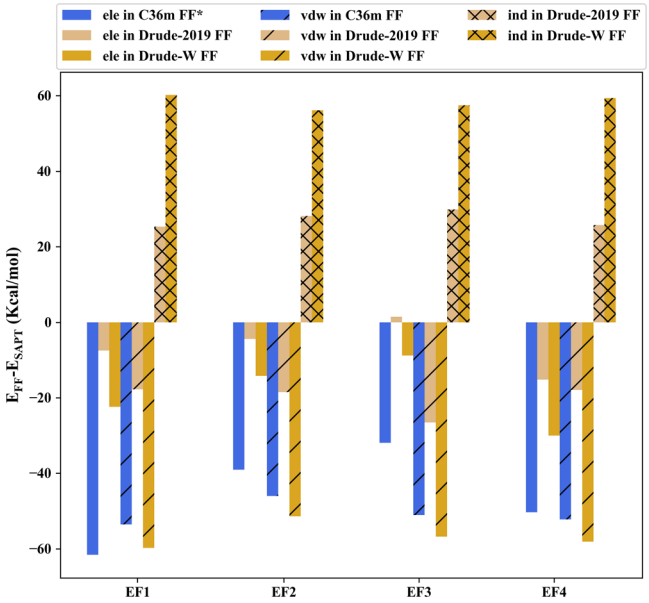

Figure 4. Comparison of each component of the binding energies between the calcium ion and the EF-hand loops (kcal/mol). The electrostatic interaction energies computed with the additive C36m FF are compared with the summation of the SAPT electrostatics and induction terms.

and the exchange components were also correlated well with the corresponding SAPT terms, while there was a systematic deviation of 27.3 kcal/mol for the induction and −17.7 kcal/mol for the exchange. There was a slight overestimation in the dispersion energies with Drude-2019, whose difference ranged between 1.8 and 3.1 kcal/mol (Figure 4). Energy decomposition analysis was also performed with the C36m FF. There is no explicit induction component due to its additive nature, so we should compare its permeant electrostatic component with the sum of the electrostatic and induction energy in SAPT as additive FFs account for the electronic polarization effects through parametrization in an average mean-field manner. As shown in Figure 4, the C36m model led to overbinding with the electrostatic interactions overestimated by about 32 to 62 kcal/mol. The deviations of the exchange and the dispersion interactions from SAPT results were also larger than those of the polarizable Drude-2019 model. Overall, we demonstrated that the Drude FF represented a significant improvement over CHARMM additive FF in describing the interaction between Ca^{2+} and CaM EF-hand loops, in terms of both total binding energy and each interaction energy component.

In addition, we performed the binding energy and energy decomposition calculations with two revised Drude FF parameter sets proposed by Amin et al.[40] In order to avoid the overpolarization between the calcium ion and Asp or Glu residues, the NBFIX and NBTHOLE parameters between Ca^{2+} and side chain oxygen in Asp/Glu that has the same atom type (OD2C2A) in the Drude FF were adjusted. In one parameter set (Drude-T), an NBTHOLE of 2.6 was added while the NBFIX value in Drude-2019 was maintained. For another

https://doi.org/10.1021/acsphyschemau.1c00039
ACS Phys. Chem Au 2022, 2, 143−155

Table 2. Binding Free Energies of the Calcium Ion to the Four EF-Hand Loops Computed with the C36m and the Drude-2019 Force Fields[a]

force field	EF1	EF2	EF3	EF4
C36m	−22.54	−18.49	−15.65	−23.49
Drude-2019	−31.09	−45.69	−44.60	−41.41
Exp.[b]	−5.32 ± 0.07	−4.63 ± 0.03	−4.58 ± 0.04	−4.05 ± 0.12

[a]Units are kcal/mol. [b]Experimental binding free energies for the four EF-hands from ref 12.

parameter set (Drude-W) both NBFIX and NBTHOLE parameters were optimized, whose values were listed in the Supporting Information Table S2. However, as shown in Figure 3 and Table S3, the Drude-T and Drude-W parameters deteriorated in reproducing the SAPT results, with MAE in binding energy changed from 4.37 to 5.30 and 17.07 kcal/mol, respectively. Based on energy decomposition calculations, the new NBFIX and NBTHOLE parameters introduced in Drude-W made the permanent electrostatic interaction more favorable, the induction significantly less favorable, the exchange much less positive, and the dispersion interaction less favorable (Figure 4).

Binding Free Energies of Ca^{2+} to CaM EF-Hand Loops

The binding energy calculations were carried out on a single structure in gas phase, so it cannot be compared with the experimental measurements on binding free energies. Explicit solvent H-REMD/FEP simulations have been carried out with the C36m and the Drude FFs to determine the ion binding free energies to each of the four EF-hand systems according to the thermodynamic cycle shown in Figure 2. As shown in Figures S1E and S2E, ΔG_2 converged well within 2 ns H-REMD simulations and were computed to be −346.90 kcal/mol and −369.97 kcal/mol with the Drude and the C36m FFs, respectively. We note that these are intrinsic hydration free energies, which are subjected to two correction terms. The first term (−25.10 kcal/mol with the Drude SWM4-NDP model and −24.58 kcal/mol with the TIP3P model) depends on the electrostatic Galvani potential at the liquid−vacuum interface,[59,60] and the second term is an entropy correction that equals 1.99 kcal/mol at 310 K and 1 atm. With these two corrections, the real hydration free energies of Ca^{2+} were computed to be −370.01 kcal/mol and −392.56 kcal/mol with the Drude polarizable and the CHARMM additive force fields at 310 K. The hydration free energy ΔG_{HFE} of Ca^{2+} obtained with the Drude FF agrees with the value (− 369.9 kcal/mol) reported by Yu et al.[59] Both compare favorably with the experimental value of −359.70 kcal/mol at 298 K.[66]

The convergence of H-REMD/FEP calculations to decouple ions from EF-hand systems was slower. Two nanosecond simulations for each λ point with the Drude-2019 FF converged ΔG_1 within 1 kcal/mol (Figure S1), while the free energy calculations with C36m FF did not fully converge after 20 ns H-REMD/FEP simulations (Figure S2). Due to the extensive computational cost, only one set of H-REMD/FEP simulations were carried out for each system. To investigate the effect of different starting conformations, three sets of 2 ns H-REMD/FEP simulations were carried out for EF3 with the Drude-2019 FF using different initial structures extracted at 5, 100, and 200 ns of the equilibrium MD trajectory. The computed ΔG_1 were −43.63, −44.63, and −44.60 kcal/mol, respectively, indicating no obvious dependence on the starting conformations.

The computed binding free energies of Ca^{2+} to the EF-hand loops were summarized in Table 2. Both of the C36m and the Drude-2019 FFs strongly overestimated the calcium affinity in EF-hand systems. On average, C36m overestimated binding affinities by 15.40 kcal/mol, and Drude-2019 overestimated them by 36.05 kcal/mol. The order of binding strength was also not correctly reproduced by either force field. For example, Ca^{2+} bind most strongly with EF1, while Drude-2019 simulations predicted that Ca^{2+} binding with EF1 was weakest among the four loops. We also performed the binding free energy calculations with the Drude-T and Drude-W parameter sets using the same FEP protocol. While the Drude-T FF led to similar binding free energies with the Drude-2019 (data not shown), the Drude-W FF even more severely overestimated the calcium affinity to CaM EF-hand loops with computed free energies being −108.6, −93.95, −90.42, and −99.50 kcal/mol, respectively.

Analysis of MD and FEP Trajectories

While the Drude-2019 polarizable FF reproduced very well the QM binding energies of calcium/EF-hand complexes, its performance in reproducing experimental binding free energies was much worse than the C36m FF. Possible explanations included that the conformations sampled in MD simulations could be far away from the experimental structural ensemble. Even if the conformations are similar, the binding energies of these conformations might not be modeled accurately by the force field. Furthermore, there are entropy changes associated with ion binding/unbinding that need to be correctly accounted for. We analyzed the 200 ns MD trajectories and the H-REMD/FEP trajectories to understand the large deviation of computed binding free energies from experimental measurements. We note that only the λ = 1 states of the H-REMD/FEP simulations were used as they corresponded to physically meaningful states, and although their lengths were relatively short they represent a large conformational space due to the enhanced sampling brought by H-REMD.

Binding Energies and Structural Deviations

We first analyzed the ensemble averaged binding energies of calcium ions to the EF-hand loops in H-REMD/FEP simulations (Figure S3). The general trend was similar to the single point calculations using the conformations from the crystal structure. The ensemble averaged binding energies from additive simulations were significantly more negative by 100 to 300 kcal/mol compared with the Drude simulations. The average binding energies computed from the Drude-2019 trajectories were −678.99, −819.48, −631.76, and −878.04 kcal/mol for the four EF-hand loops, respectively. They were slightly more negative than the single point binding energies presented in Table 1.

We note that one source of discrepancy might be due to the difference between the model systems used in the FEP simulations and the experimental systems in which the EF-hand loops were grafted on the protein CD2. To shed light on

https://doi.org/10.1021/acsphyschemau.1c00039
ACS Phys. Chem Au 2022, 2, 143−155

such differences, we constructed four simulation systems with the EF-hand loops grafted on the domain 1 of CD2 and carried out 30 ns MD simulations with the C36m and the Drude-2019 FFs for these CD2-EF-hand systems, respectively (methods included in Supporting Information). The interaction energies between calcium ions and the EF-hand loops were extracted from MD trajectories and compared with the EF-hand alone systems (Figure S4). While the distributions of interaction energies were similar in some systems such as the EF1 loop modeled with the Drude FF, large deviations were observed in systems such as the EF2 loop modeled with C36m, indicating that the existence of CD2 can interfere with Ca^{2+} binding to EF-hand loops.

We also analyzed the root-mean-square deviations (RMSDs) of the EF-hand loops with respect to the crystal structure along with the H-REMD/FEP simulations. Both $\lambda = 1$ and $= 0$ states were used, as they represented the ion-bound and the ion-unbound states, and we note that no restraints on EF-hand loops were used in the simulations. With the C36m force field, the EF-hand loops were very stable with calcium ion binding as indicated by RMSDs being around 3 Å (Figure S5). Unbinding of Ca^{2+} induced large conformational changes of the peptides, as the RMSDs increased to 7 Å or larger. For the simulations with Drude-2019, the RMSDs of both Ca^{2+}-bound and Ca^{2+}-unbound EF-hands were around 4 to 5 Å compared with the crystal structure (Figure S6, and similar for the simulations with Drude-W as shown in Figure S7). The conformational entropies of ion-unbound states might be underestimated with the Drude simulations, which made the binding free energy more negative than it was supposed to be.

Calcium Coordination

The RMSDs of ion-bound states indicated that the EF-hand loops were closer to the experimental structure in the C36m simulations than in the Drude simulations. We further characterized the local structures around the calcium ion by computing their coordination numbers, which partially correlate with the binding energies between the calcium ion and EF-hand loops. In the crystal structure, calcium's coordination had almost the same pentagonal bipyramid structure in each of the four calcium/EF-hand complexes. With the calcium ion at the center, the side chain's terminal O atoms in the third (Asp) and the fifth residue (Asp or Asn), backbone oxygen in the seventh residue, and two O atoms of carbonyl in the last residue (Glu) form a coplanar pentagon. In addition, the O atoms from the terminus of the first residue (Asp) and coordinated water were the two vertexes locating two sides of the pentagon plane, respectively. Therefore, the coordination numbers are 7.

The coordination numbers from MD trajectories were computed as the ensemble average of the number of heavy atoms that were within 3.0 Å of the calcium ion, and listed in Table 3. The final configurations of the 200 ns MD trajectories generated with the C36m and the Drude-2019 FFs for the four complexes were shown in Figure 5. As shown in Table 3, coordination numbers calculated from the 200 ns MD simulations and the 2 ns H-REMD/FEP trajectories were very similar. The coordination numbers with the C36m FF equaled or were slightly over 7, while those with the Drude-2019 model were also close to or slightly less than 7.

The final configuration of the Ca^{2+}/EF1 complex along the C36m MD trajectory was almost the same as that in the crystal structure (Figure 5A and B). The small fluctuation of the coordination number was mainly due to the motion of the coordinated water molecule and the coordination transition between the two side-chain oxygen atoms of Asp20 (Figure S8). Detailed analyses on the calcium coordination of the C36m simulations were presented in the Supporting Information Figures S8−S11. The average calcium coordination number of the EF3 was 7.4 as the side chain of Asp93 switched between monodentate and bidentate coordination modes (Figure S10).

Table 3. Coordination Numbers of Calcium for the Four Individual EF-Hand Loops

		EF1	EF2	EF3	EF4
MD	C36m	7.0 ± 0.1	7.2 ± 0.2	7.4 ± 0.3	7.1 ± 0.2
	Drude-2019	6.6 ± 0.3	6.7 ± 0.3	6.8 ± 0.2	6.9 ± 0.2
	Drude-2019 (oxygen only)	6.6 ± 0.3	6.2 ± 0.3	5.9 ± 0.2	6.4 ± 0.3
FEP	C36m	7.0 ± 0.1	7.1 ± 0.2	7.1 ± 0.1	7.0 ± 0.1
	Drude-2019	6.6 ± 0.3	6.9 ± 0.2	6.9 ± 0.1	7.2 ± 0.2
	Drude-2019 (oxygen only)	6.6 ± 0.3	5.9 ± 0.2	6.0 ± 0.1	6.2 ± 0.2

For the Drude-2019 simulations, although the coordination numbers were also close to 7, a careful examination (Figures S12−S16) revealed that the coordination included nitrogen atoms in the EF2, EF3, and EF4 complexes. The coordination numbers decrease to about 6 if only oxygen atoms were included in the calculation. Commonly, one initially bound aspartic acid residue (Asp58 in EF2, Asp95 in EF3, and Asp133 in EF4) detached from the calcium ion, and the nitrogen atom in the nearby Asn/Gln residues (Asn60 in EF2, Asn97 in EF3, and Gln135 in EF4) moved closer to keep 7 coordination through monodentate or bidentate modes, as illustrated in Figure 5F, I, and L. We note that coordinated nitrogen atoms were not observed in configurations from C36m FF and also barely existed in other known calcium binding proteins. The same phenomenon was observed in the simulations with the Drude-W parameter set (Figures S17−S20), and the Drude-W model failed to reproduce the coordination of a Ca^{2+}-bound water molecule in all EF-hand loops, which further reduced the calcium coordination numbers. The coordination numbers were computed to be 5.4 ± 0.4, 5.4 ± 0.4, 5.2 ± 0.3, and 5.8 ± 0.3, respectively, using the H-REMD/FEP trajectories with the Drude-W model if only oxygen atoms were counted.

Induced Dipole Moments

The distances between Ca^{2+} and the side chain nitrogen and carbon atoms of the Asn/Gln residues can be shorter than 3.0 Å during MD simulations with the Drude-2019 FF, as evident in Figures S13D, S14E, S15F, and S16. We further investigated the induced dipole moments of these atoms. In the Drude simulations, a hardwall constraint[33] of 0.25 Å was applied to limit the distance between the parent atom and its Drude particle, which effectively caps their induced dipole moments. The threshold of the induced dipole moments for the calcium ion and its coordinated atoms are listed in Table S4, and they can be compared with instant induced dipoles (Figures 6 and 7) to check whether there are overpolarization effects in the simulations.

As shown in Figure 6, the induced dipole moments of side chain nitrogen atoms for Asn60, Asn97, and Gln135 that have the same atom type (ND2A1) hit the threshold (2.73 D)

https://doi.org/10.1021/acsphyschemau.1c00039
ACS Phys. Chem Au 2022, 2, 143−155

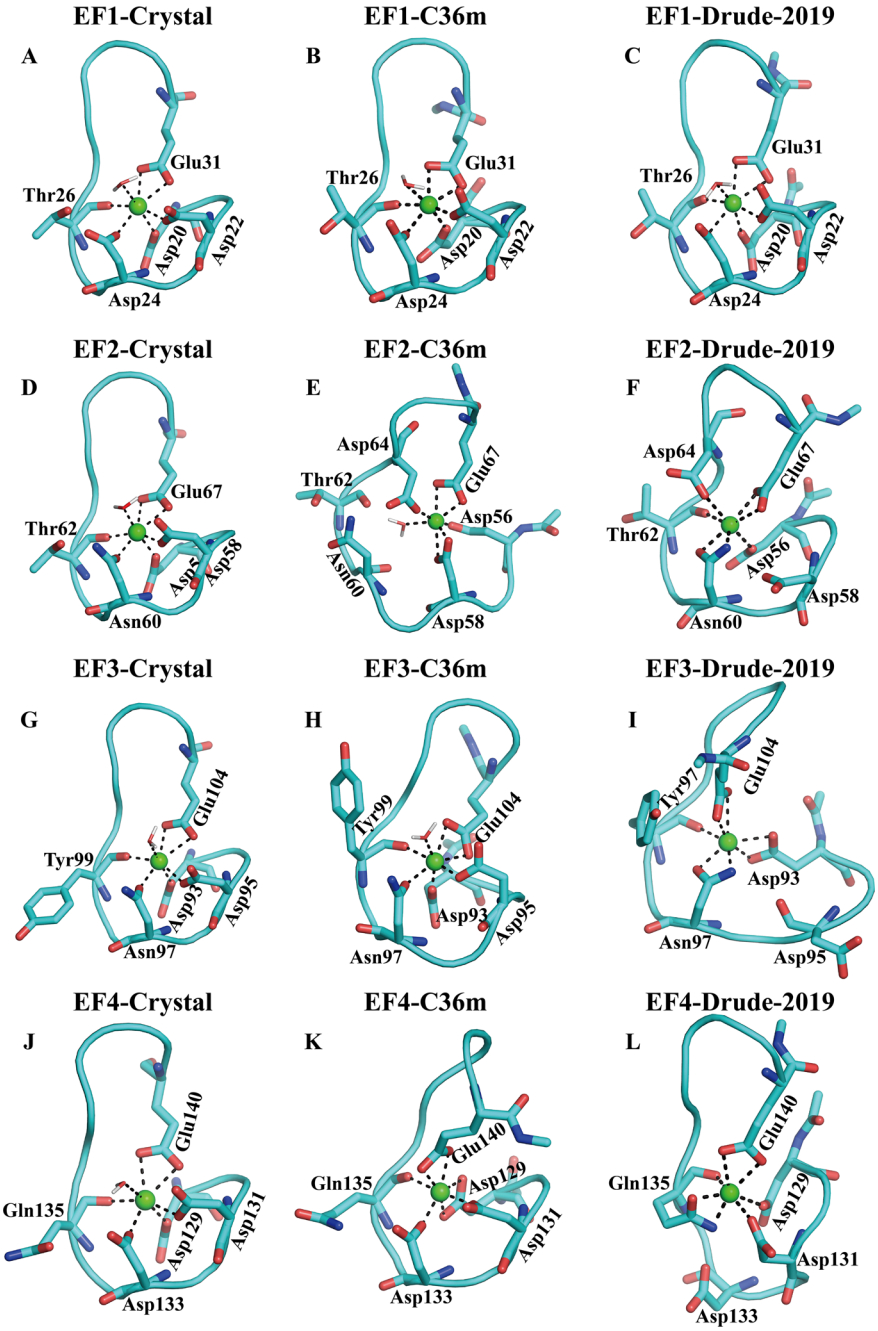

Figure 5. Structures of Ca^{2+} bound with EF1 (A), EF2 (D), EF3 (G), and EF4 (J) from the crystal structure, with EF1 (B), EF2 (E), EF3 (H), and EF4 (K) from the MD trajectories's final snapshots with C36m force field, and with EF1 (C), EF2 (F), EF3 (I), and EF4 (L) from the MD trajectories's final snapshots with Drude-2019 force field.

during the 200 ns MD simulations with the Drude-2019 FF. As the final configurations were used in the free energy calculations, such overpolarization effects were maintained throughout the H-REMD/FEP simulations (Figure 7). Improvement in the Drude force field would be needed to avoid the Drude particles frequently hitting the hardwall constraints,[39] which in this case would be the reparameterization of the interaction parameters between Ca^{2+} and the ND2A1 atom type. It is interesting to note that the overpolarization was manifested in their connecting atoms, resulting in the increase of induced dipole moments of the side-chain carbon atoms in Asn/Gln that sometimes also reached their threshold value of 2.62 D (Figure 6).

We examined the induced dipole moments of all possible coordinated atoms along the 200 ns MD and the 2 ns H-REMD/FEP simulations with the Drude-2019 FF (Supporting Information Figures S23−S31) and found that the induced dipole moments of all coordinated oxygen atoms were lower than the threshold values. In very rare cases the dipole moments of carboxyl oxygen atoms of Glu were close to their threshold value (1.74 D) in MD simulations (Figure S23). With the Drude-W parameter set, the overpolarization effects on the side chain nitrogen atoms in Asn/Gln were also observed, while the induced dipole moments of side chain carboxyl carbon atoms of Asp/Glu also frequently reached their threshold value of 2.10 D (Figures S21 and S22).

https://doi.org/10.1021/acsphyschemau.1c00039
ACS Phys. Chem Au 2022, 2, 143−155

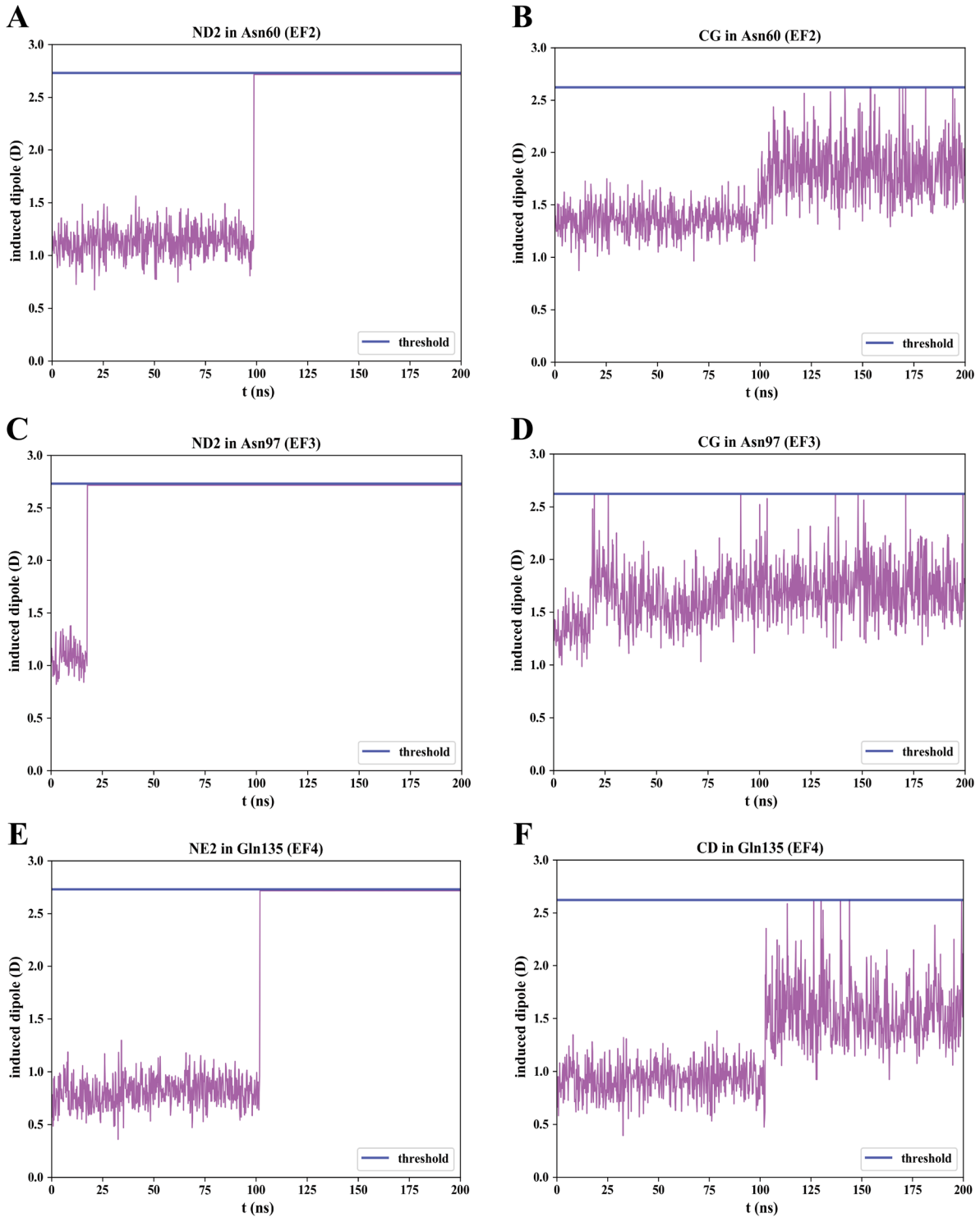

Figure 6. Dipole moments of side chain carbon and nitrogen atoms for Asn and Gln in the MD simulations with the Drude-2019 force field.

The total dipole moments of the side chain and the backbone of Ca^{2+}-coordinated residues were computed along the Drude trajectories, as such analysis has been used to provide physical insights in peptide dynamics.[67,68] Increases in the side chain dipole moments of Asn60 (EF2), Asn97 (EF3), and Gln135 (EF4) were observed in 200 ns MD simulations with the Drude-2019 FF (Figure S32), in accordance with the increase in the induced dipole of individual side chain atoms (Figure 6). Comparison of residue dipole moments with (λ = 1) and without (λ = 0) Ca^{2+} binding showed that the calcium ion can induce strong polarization effects on the side chains but much weaker on the peptide backbones (Figures S33 and S34).

DISCUSSIONS AND CONCLUSION

The Drude polarizable force fields have been widely used to understand the peptide folding cooperativity,[67] partitioning of small molecules,[69,70] ligand−protein binding dynamics,[71] and interficial properties.[72] A key motivation of this study was to compare simulations with the experimental measurement on

https://doi.org/10.1021/acsphyschemau.1c00039
ACS Phys. Chem Au 2022, 2, 143−155

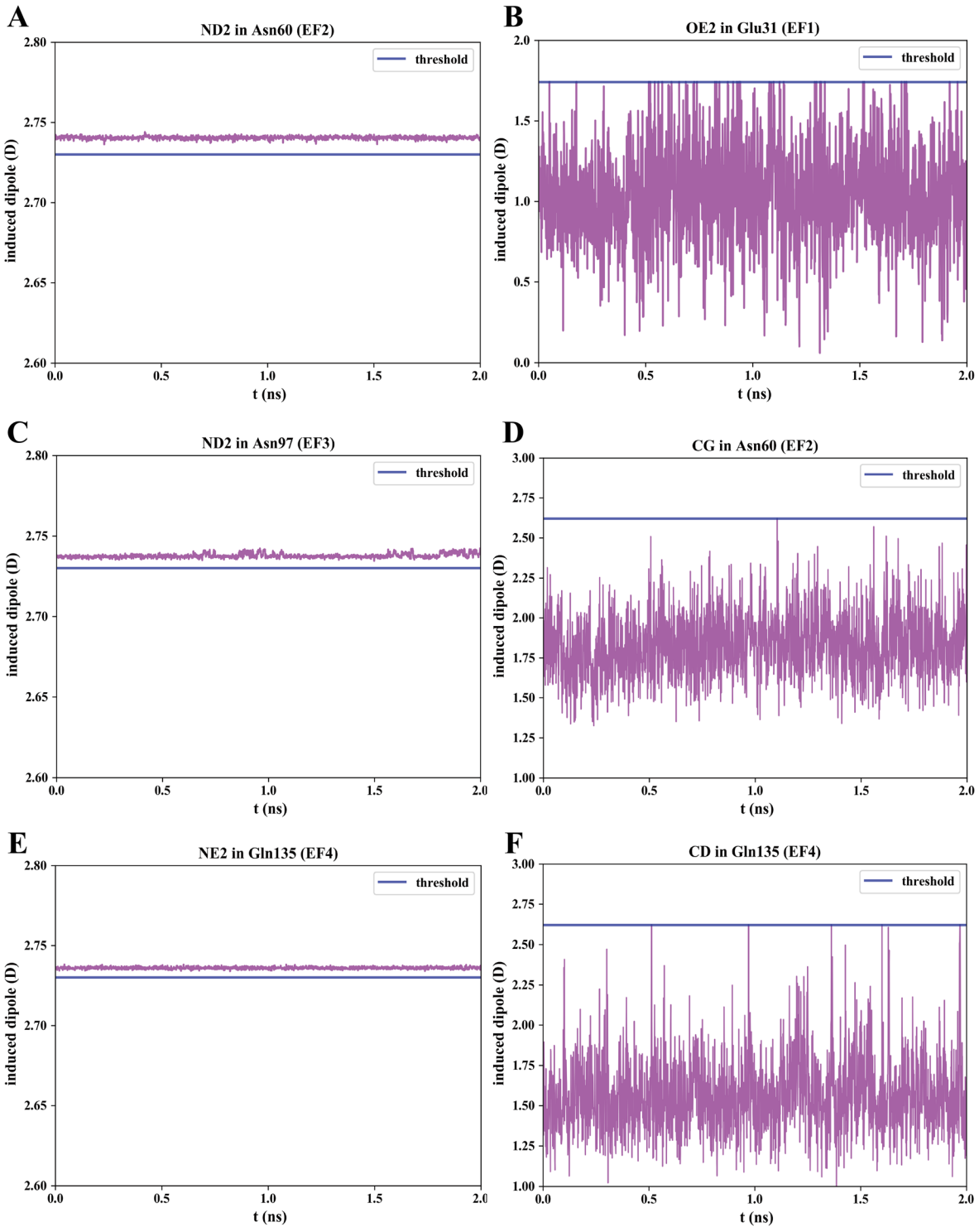

Figure 7. Dipole moments of side chain oxygen, carbon, and nitrogen atoms for Asp, Glu, Asn, and Gln in the H-REMD/FEP simulations with the Drude-2019 force field.

the binding free energies between calcium ion and the EF-hand loops. We first compared the binding energies using the experimentally determined complex structures, and found out that the polarizable Drude-2019 FF reproduced the SAPT calculation results, both in terms of total interaction energies as well as each component of the interaction energies including electrostatic, induction, exchange, and dispersion terms. However, large deviations of the binding free energies from the experimental values were obtained with FEP simulations employing the Drude-2019 FF. Detailed analysis indicated that one of the main reasons might be that the calcium coordination geometries were distorted with the Drude FFs, including both the Drude-2019 and the recently proposed Drude-T and Drude-W parameter sets.[40]

In the crystal structure of Calmodulin, all the calcium/EF-hand complexes have the same set of 7 coordinated atoms on the calcium ion: 1 side chain oxygen atom of residues 1, 3, and 5; 1 backbone oxygen atom of residue 7; 2 side chain oxygen

https://doi.org/10.1021/acsphyschemau.1c00039
ACS Phys. Chem Au 2022, 2, 143−155

atoms of residue 12; and 1 oxygen atom of a water molecule. While the coordination numbers remained close to 7 in the Drude-2019 simulations, the coordinated atoms included side chain nitrogen atoms of Asn/Gln residues. The strong interactions between Ca^{2+} and the nitrogen atoms were associated with the overpolarization of these atoms. We note that a high frequency of Drude particles hitting the hardwalls violates the adiabatic nature of polarization response, which compromises the validity of FEP calculations. Therefore, FF refinement by introducing NBFIX and NBTHOLE terms between Ca^{2+} and the ND2A1 atom type in the Drude FF is expected to improve the modeling of the dynamics and thermodynamics of Ca^{2+}/EF-hand systems.

The coordination modes of residues to the calcium ion are still controversial. In the high-resolution crystal structures of CaM, two coordination modes were found as bidentate for glutamic acids and monodentate for aspartic acids.[42] For the binding mode of glutamic acids, both the additive C36m and the polarizable Drude FFs showed that the bidentate mode was favored during simulations. The same observation was made by the scaled-charge ECCR model.[15] For the binding mode of aspartic acids, additive force fields typically predicted bidentate coordination, while polarizable models suggested mainly monodentate.[15,40] In our C36m simulations, aspartic acids can form both monodentate and bidentate coordination, and transitions between these two modes were observed in tens or hundreds of nanoseconds (Figures S8−S10). Most of the Asp residues in our Drude-2019 simulations were in monodentate binding mode, with an exception of Asp93 in the EF3. Recently, Oliveira et al. obtained the free energy profile along with carboxylate carbon−cation distance for the calcium ion, and showed that Ca^{2+} were equally stable in monodentate and bidentate geometries.[73] More relevant experiments as well as computational studies with accurate models are needed to investigate the binding modes of amino acid residues to the calcium ions.

A recent study of the same Ca^{2+}/EF-hand systems by Zhang et al.[74] showed that the polarization and charge transfer effects occur not only in the coordinating residues but also for the residues that are not actively involved in Ca^{2+} coordination. They also showed that the water molecule was important to maintain the pentagonal bipyramidal geometry. In our work, we found no water molecule coordinated with the calcium ion in the Drude-2019 force field, possibly due to the excessively strong interactions between Ca^{2+} and side chain nitrogen atoms of Asn/Gln residues. It would be interesting to see whether the finetuning of this type of interaction would lead to significantly better description of the structure and thermodynamics of calcium binding to CaM EF-hand loops. Our work demonstrated that the Ca^{2+}/EF-hand systems are useful and challenging model systems to test the accuracy of force field models for metal ions and ion binding sites in proteins.

■ ASSOCIATED CONTENT

Supporting Information

The Supporting Information is available free of charge at https://pubs.acs.org/doi/10.1021/acsphyschemau.1c00039.

Tables of amino acid sequences for the four calcium-binding loops of CaM, parameters of calcium ion in Drude-2019, Drude-T, and Drude-W force field, the interaction energies and energy components for the binding of the calcium ion with four EF-hand loops in Drude-T and Drude-W force fields, and the threshold of the induced dipole moments for calcium ion and coordinated atoms are listed. Figures of free energy differences for Ca^{2+}/EF1, Ca^{2+}/EF2, Ca^{2+}/EF3, Ca^{2+}/EF4, and Ca^{2+} in bulk water with C36m and Drude-2019, the binding energy of calcium ion to the four EF-hand loops in H-REMD/FEP simulations with C36m, Drude-2019, and Drude-W force fields, the RMSDs of EF-hand loops with respect to their crystal structure in H-REMD/FEP simulations with C36m, Drude-2019, and Drude-W force fields, the distance between calcium ion and coordinated atoms in MD and H-REMD/FEP simulations with C36m, Drude-2019, and Drude-W force fields, the induced dipole moments of coordinated atoms in MD and H-REMD/FEP simulations with Drude-2019 and Drude-W force fields, and the dipole moments of coordinated residues in MD and H-REMD/FEP simulations with Drude-2019 force field are provided (PDF)

■ AUTHOR INFORMATION

Corresponding Author

Jing Huang − *Key Laboratory of Structural Biology of Zhejiang Province, School of Life Sciences, Westlake University, Hangzhou 310024 Zhejiang, China; Westlake AI Therapeutics Lab, Westlake Laboratory of Life Sciences and Biomedicine, Hangzhou 310024 Zhejiang, China; Institute of Biology, Westlake Institute for Advanced Study, Hangzhou 310024 Zhejiang, China;* orcid.org/0000-0001-9639-2907; Email: huangjing@westlake.edu.cn

Authors

Qiaozhu Tan − *College of Life Sciences, Zhejiang University, Hangzhou 310058 Zhejiang, China; Key Laboratory of Structural Biology of Zhejiang Province, School of Life Sciences, Westlake University, Hangzhou 310024 Zhejiang, China; Westlake AI Therapeutics Lab, Westlake Laboratory of Life Sciences and Biomedicine, Hangzhou 310024 Zhejiang, China*

Ye Ding − *College of Life Sciences, Zhejiang University, Hangzhou 310058 Zhejiang, China; Key Laboratory of Structural Biology of Zhejiang Province, School of Life Sciences, Westlake University, Hangzhou 310024 Zhejiang, China; Westlake AI Therapeutics Lab, Westlake Laboratory of Life Sciences and Biomedicine, Hangzhou 310024 Zhejiang, China*

Zongyang Qiu − *Key Laboratory of Structural Biology of Zhejiang Province, School of Life Sciences, Westlake University, Hangzhou 310024 Zhejiang, China; Westlake AI Therapeutics Lab, Westlake Laboratory of Life Sciences and Biomedicine, Hangzhou 310024 Zhejiang, China; Institute of Biology, Westlake Institute for Advanced Study, Hangzhou 310024 Zhejiang, China*

Complete contact information is available at: https://pubs.acs.org/10.1021/acsphyschemau.1c00039

Notes

The authors declare no competing financial interest.

■ ACKNOWLEDGMENTS

We thank Westlake University Supercomputer Center for computational resources and related assistance. We thank

Houhou Huang for helpful discussions. The work is supported by the National Natural Science Foundation of China (Grant No. 21803057, 32171247), by the Zhejiang Provincial Natural Science Foundation of China (Grant No. LR19B030001), and by China Postdoctoral Science Foundation (Grant No. 2020M681934).

REFERENCES

(1) Giorgi, C.; Marchi, S.; Pinton, P. The machineries, regulation and cellular functions of mitochondrial calcium. *Nat. Rev. Mol. Cell Biol.* **2018**, *19*, 713−730.
(2) Clapham, D. E. Calcium signaling. *Cell* **2007**, *131*, 1047−1058.
(3) Osawa, M.; Tokumitsu, H.; Swindells, M. B.; Kurihara, H.; Orita, M.; Shibanuma, T.; Furuya, T.; Ikura, M. A novel target recognition revealed by calmodulin in complex with Ca 2+-calmodulin-dependent kinase kinase. *Nat. Struct. Biol.* **1999**, *6*, 819−824.
(4) Means, A. R. Calcium, calmodulin and cell cycle regulation. *FEBS Lett.* **1994**, *347*, 1−4.
(5) Neuhaus, G.; Bowler, C.; Kern, R.; Chua, N.-H. Calcium/calmodulin-dependent and-independent phytochrome signal transduction pathways. *Cell* **1993**, *73*, 937−952.
(6) Jiang, X.; Li, J.; Paskind, M.; Epstein, P. Inhibition of calmodulin-dependent phosphodiesterase induces apoptosis in human leukemic cells. *Proc. Natl. Acad. Sci. U. S. A.* **1996**, *93*, 11236−11241.
(7) Gifford, J. L.; Walsh, M. P.; Vogel, H. J. Structures and metal-ion-binding properties of the Ca2+-binding helix−loop−helix EF-hand motifs. *Biochem. J.* **2007**, *405*, 199−221.
(8) Grabarek, Z. Structural basis for diversity of the EF-hand calcium-binding proteins. *J. Mol. Biol.* **2006**, *359*, 509−525.
(9) Abzhanov, A.; Kuo, W. P.; Hartmann, C.; Grant, B. R.; Grant, P. R.; Tabin, C. J. The calmodulin pathway and evolution of elongated beak morphology in Darwin's finches. *Nature* **2006**, *442*, 563−567.
(10) Stigler, J.; Ziegler, F.; Gieseke, A.; Gebhardt, J. C. M.; Rief, M. The complex folding network of single calmodulin molecules. *Science* **2011**, *334*, 512−516.
(11) Stigler, J.; Rief, M. Calcium-dependent folding of single calmodulin molecules. *Proc. Natl. Acad. Sci. U. S. A.* **2012**, *109*, 17814−17819.
(12) Ye, Y.; Lee, H.-W.; Yang, W.; Shealy, S.; Yang, J. J. Probing site-specific calmodulin calcium and lanthanide affinity by grafting. *J. Am. Chem. Soc.* **2005**, *127*, 3743−3750.
(13) Lepšík, M.; Field, M. J. Binding of calcium and other metal ions to the EF-hand loops of calmodulin studied by quantum chemical calculations and molecular dynamics simulations. *J. Phys. Chem. B* **2007**, *111*, 10012−10022.
(14) Chen, C.; Huang, Y.; Jiang, X.; Xiao, Y. Binding free-energy calculation of an ion-peptide complex by constrained dynamics. *Phys. Rev. E* **2013**, *87*, 062−705.
(15) Kohagen, M.; Lepsik, M.; Jungwirth, P. Calcium binding to calmodulin by molecular dynamics with effective polarization. *J. Phys. Chem. Lett.* **2014**, *5*, 3964−3969.
(16) Basit, A.; Mishra, R. K.; Bandyopadhyay, P. Calcium ion binding to calmodulin: binding free energy calculation using the molecular mechanics Poisson-Boltzmann surface area (MM-PBSA) method by incorporating implicit polarization. *J. Biomol. Struct. Dyn.* **2021**, *39*, 7213.
(17) Kohagen, M.; Mason, P. E.; Jungwirth, P. Accurate description of calcium solvation in concentrated aqueous solutions. *J. Phys. Chem. B* **2014**, *118*, 7902−7909.
(18) Li, P.; Merz, K. M., Jr Taking into account the ion-induced dipole interaction in the nonbonded model of ions. *J. Chem. Theory Comput.* **2014**, *10*, 289−297.
(19) Li, P.; Song, L. F.; Merz, K. M., Jr Systematic parameterization of monovalent ions employing the nonbonded model. *J. Chem. Theory Comput.* **2015**, *11*, 1645−1657.
(20) Li, P.; Song, L. F.; Merz, K. M., Jr Parameterization of highly charged metal ions using the 12−6-4 LJ-type nonbonded model in explicit water. *J. Phys. Chem. B* **2015**, *119*, 883−895.
(21) Saxena, A.; Sept, D. Multisite ion models that improve coordination and free energy calculations in molecular dynamics simulations. *J. Chem. Theory Comput.* **2013**, *9*, 3538−3542.
(22) Zhang, A.; Yu, H.; Liu, C.; Song, C. The Ca2+ permeation mechanism of the ryanodine receptor revealed by a multi-site ion model. *Nat. Commun.* **2020**, *11*, 1−10.
(23) Leontyev, I.; Stuchebrukhov, A. Accounting for electronic polarization in non-polarizable force fields. *Phys. Chem. Chem. Phys.* **2011**, *13*, 2613−2626.
(24) Leontyev, I. V.; Stuchebrukhov, A. A. Polarizable mean-field model of water for biological simulations with AMBER and CHARMM force fields. *J. Chem. Theory Comput.* **2012**, *8*, 3207−3216.
(25) Ponder, J. W.; Wu, C.; Ren, P.; Pande, V. S.; Chodera, J. D.; Schnieders, M. J.; Haque, I.; Mobley, D. L.; Lambrecht, D. S.; DiStasio, R. A.; Head-Gordon, M.; Clark, G. N. I.; Johnson, M. E.; Head-Gordon, T. Current status of the AMOEBA polarizable force field. *J. Phys. Chem. B* **2010**, *114*, 2549−2564.
(26) Yu, W.; Lopes, P. E.; Roux, B.; MacKerell, A. D., Jr Six-site polarizable model of water based on the classical Drude oscillator. *J. Chem. Phys.* **2013**, *138*, 034508.
(27) Ren, P.; Ponder, J. W. Polarizable atomic multipole water model for molecular mechanics simulation. *J. Phys. Chem. B* **2003**, *107*, 5933−5947.
(28) Ren, P.; Wu, C.; Ponder, J. W. Polarizable Atomic Multipole-Based Molecular Mechanics for Organic Molecules. *J. Chem. Theory Comput.* **2011**, *7*, 3143−3161.
(29) Shi, Y.; Xia, Z.; Zhang, J.; Best, R.; Wu, C.; Ponder, J. W.; Ren, P. Polarizable Atomic Multipole-Based AMOEBA Force Field for Proteins. *J. Chem. Theory Comput.* **2013**, *9*, 4046−4063.
(30) Lopes, P.; Huang, J.; Shim, J.; Luo, Y.; Li, H.; Roux, B.; MacKerell, A. Polarizable Force Field for Peptides and Proteins Based on the Classical Drude Oscillator. *J. Chem. Theory Comput.* **2013**, *9*, 5430−5449.
(31) Huang, J.; Lopes, P.; Roux, B.; MacKerell, A. Recent Advances in Polarizable Force Fields for Macromolecules: Microsecond Simulations of Proteins Using the Classical Drude Oscillator Model. *J. Phys. Chem. Lett.* **2014**, *5*, 3144−3150.
(32) Savelyev, A.; MacKerell, A. D. All-atom polarizable force field for DNA based on the classical drude oscillator model. *J. Comput. Chem.* **2014**, *35*, 1219−1239.
(33) Chowdhary, J.; Harder, E.; Lopes, P. E.; Huang, L.; MacKerell, A. D., Jr; Roux, B. A polarizable force field of dipalmitoylphosphatidylcholine based on the classical drude model for molecular dynamics simulations of lipids. *J. Phys. Chem. B* **2013**, *117*, 9142−9160.
(34) Peng, X.; Zhang, Y.; Chu, H.; Li, Y.; Zhang, D.; Cao, L.; Li, G. Accurate evaluation of ion conductivity of the gramicidin a channel using a polarizable force field without any corrections. *J. Chem. Theory Comput.* **2016**, *12*, 2973−2982.
(35) Huang, J.; Simmonett, A. C.; Pickard, F. C.; MacKerell, A. D.; Brooks, B. R. Mapping the Drude Polarizable Force Field onto a Multipole and Induced Dipole Model. *J. Chem. Phys.* **2017**, *147*, 161702.
(36) Jing, Z.; Qi, R.; Liu, C.; Ren, P. Study of interactions between metal ions and protein model compounds by energy decomposition analyses and the AMOEBA force field. *J. Chem. Phys.* **2017**, *147*, 161733.
(37) Jing, Z.; Liu, C.; Qi, R.; Ren, P. Many-body effect determines the selectivity for Ca2+ and Mg2+ in proteins. *Proc. Natl. Acad. Sci. U. S. A.* **2018**, *115*, E7495−E7501.
(38) Li, H.; Ngo, V.; Da Silva, M. C.; Salahub, D. R.; Callahan, K.; Roux, B.; Noskov, S. Y. Representation of ion−protein interactions using the drude polarizable force-field. *J. Phys. Chem. B* **2015**, *119*, 9401−9416.
(39) Lin, F.-Y.; Huang, J.; Pandey, P.; Rupakheti, C.; Li, J.; Roux, B.; MacKerell, A. D. Further Optimization and Validation of the Classical

Drude Polarizable Protein Force Field. *J. Chem. Theory Comput.* **2020**, *16*, 3221−3239.
(40) Amin, K. S.; Hu, X.; Salahub, D. R.; Baldauf, C.; Lim, C.; Noskov, S. Benchmarking polarizable and non-polarizable force fields for Ca2+−peptides against a comprehensive QM dataset. *J. Chem. Phys.* **2020**, *153*, 144102.
(41) Huang, J.; Rauscher, S.; Nawrocki, G.; Ran, T.; Feig, M.; de Groot, B. L.; Grubmueller, H.; MacKerell, A. CHARMM36m: An Improved Force Field for Folded and Intrinsically Disordered Proteins. *Nat. Methods* **2017**, *14*, 71−73.
(42) Chattopadhyaya, R.; Meador, W. E.; Means, A. R.; Quiocho, F. A. Calmodulin structure refined at 1.7 Å resolution. *J. Mol. Biol.* **1992**, *228*, 1177−1192.
(43) Becke, A. D. Density-functional thermochemistry. III. The role of exact exchange. *J. Chem. Phys.* **1993**, *98*, 5648.
(44) Stephens, P. J.; Devlin, F. J.; Chabalowski, C. F.; Frisch, M. J. Ab initio calculation of vibrational absorption and circular dichroism spectra using density functional force fields. *J. Phys. Chem.* **1994**, *98*, 11623−11627.
(45) Lee, C.; Yang, W.; Parr, R. G. Development of the Colle-Salvetti correlation-energy formula into a functional of the electron density. *Phys. Rev. B: Condens. Matter Mater. Phys.* **1988**, *37*, 785.
(46) Frisch, M. J. et al. *Gaussian 16*, Revision C.01. 2016; Gaussian Inc.: Wallingford, CT.
(47) Boys, S. F.; Bernardi, F. The calculation of small molecular interactions by the differences of separate total energies. Some procedures with reduced errors. *Mol. Phys.* **1970**, *19*, 553−566.
(48) Parrish, R. M.; et al. Psi4 1.1: An open-source electronic structure program emphasizing automation, advanced libraries, and interoperability. *J. Chem. Theory Comput.* **2017**, *13*, 3185−3197.
(49) Jorgensen, W. L.; Chandrasekhar, J.; Madura, J. D.; Impey, R. W.; Klein, M. L. Comparison of simple potential functions for simulating liquid water. *J. Chem. Phys.* **1983**, *79*, 926−935.
(50) Lamoureux, G.; Harder, E.; Vorobyov, I. V.; Roux, B.; MacKerell, A. D., Jr A polarizable model of water for molecular dynamics simulations of biomolecules. *Chem. Phys. Lett.* **2006**, *418*, 245−249.
(51) Darden, T.; York, D.; Pedersen, L. Particle mesh Ewald: An N·log (N) method for Ewald sums in large systems. *J. Chem. Phys.* **1993**, *98*, 10089−10092.
(52) Van Gunsteren, W.; Berendsen, H. J. Algorithms for macromolecular dynamics and constraint dynamics. *Mol. Phys.* **1977**, *34*, 1311−1327.
(53) Andersen, H. C. Molecular dynamics simulations at constant pressure and/or temperature. *J. Chem. Phys.* **1980**, *72*, 2384−2393.
(54) Lamoureux, G.; Roux, B. Modeling induced polarization with classical Drude oscillators: Theory and molecular dynamics simulation algorithm. *J. Chem. Phys.* **2003**, *119*, 3025−3039.
(55) Åqvist, J.; Wennerström, P.; Nervall, M.; Bjelic, S.; Brandsdal, B. O. Molecular dynamics simulations of water and biomolecules with a Monte Carlo constant pressure algorithm. *Chem. Phys. Lett.* **2004**, *384*, 288−294.
(56) Brooks, B. R.; Bruccoleri, R. E.; Olafson, B. D.; States, D. J.; Swaminathan, S.; Karplus, M. CHARMM: A Program for Macromolecular Energy, Minimization, and Dynamics Calculations. *J. Comput. Chem.* **1983**, *4*, 187−217.
(57) Brooks, B. R.; et al. CHARMM: the biomolecular simulation program. *J. Comput. Chem.* **2009**, *30*, 1545−1614.
(58) Eastman, P.; Swails, J.; Chodera, J. D.; McGibbon, R. T.; Zhao, Y.; Beauchamp, K. A.; Wang, L.-P.; Simmonett, A. C.; Harrigan, M. P.; Stern, C. D.; Wiewiora, R. P.; Brooks, B. R.; Pande, V. S. OpenMM 7: Rapid development of high performance algorithms for molecular dynamics. *PLoS Comput. Biol.* **2017**, *13*, No. e1005659.
(59) Yu, H.; Whitfield, T. W.; Harder, E.; Lamoureux, G.; Vorobyov, I.; Anisimov, V. M.; MacKerell, A. D., Jr; Roux, B. Simulating monovalent and divalent ions in aqueous solution using a Drude polarizable force field. *J. Chem. Theory Comput.* **2010**, *6*, 774−786.
(60) Zhang, H.; Yin, C.; Jiang, Y.; van der Spoel, D. Force field benchmark of amino acids: I. hydration and diffusion in different water models. *J. Chem. Inf. Model.* **2018**, *58*, 1037−1052.
(61) Sugita, Y.; Kitao, A.; Okamoto, Y. Multidimensional replica-exchange method for free-energy calculations. *J. Chem. Phys.* **2000**, *113*, 6042−6051.
(62) Nosé, S. A unified formulation of the constant temperature molecular dynamics methods. *J. Chem. Phys.* **1984**, *81*, 511−519.
(63) Hoover, W. G. Canonical dynamics: Equilibrium phase-space distributions. *Phys. Rev. A: At., Mol., Opt. Phys.* **1985**, *31*, 1695.
(64) Shirts, M. R.; Chodera, J. D. Statistically optimal analysis of samples from multiple equilibrium states. *J. Chem. Phys.* **2008**, *129*, 124105.
(65) Klimovich, P. V.; Shirts, M. R.; Mobley, D. L. Guidelines for the analysis of free energy calculations. *J. Comput.-Aided Mol. Des.* **2015**, *29*, 397−411.
(66) Marcus, Y. Thermodynamics of solvation of ions. Part 5. Gibbs free energy of hydration at 298.15 K. *J. Chem. Soc., Faraday Trans.* **1991**, *87*, 2995−2999.
(67) Huang, J.; MacKerell, A. Induction of Peptide Bond Dipoles Drives Cooperative Helix Formation in the $(AAQAA)_3$ Peptide. *Biophys. J.* **2014**, *107*, 991−997.
(68) Lemkul, J.; Huang, J.; MacKerell, A. Induced Polarization Influences the Folded and Unfolded Conformational Ensembles of Wild-Type and Mutant Amyloid β-Peptides. *J. Phys. Chem. B* **2015**, *119*, 15574−15582.
(69) Huang, J.; Mei, Y.; König, G.; Simmonett, A. C.; Pickard, F. C.; Wu, Q.; Wang, L.-P.; MacKerell, A. D.; Brooks, B. R.; Shao, Y. An Estimation of Hybrid Quantum Mechanical Molecular Mechanical Polarization Energies for Small Molecules Using Polarizable Force-Field Approaches. *J. Chem. Theory Comput.* **2017**, *13*, 679−695.
(70) Ding, Y.; Xu, Y.; Qian, C.; Chen, J.; Zhu, J.; Huang, H.; Shi, Y.; Huang, J. Predicting partition coefficients of drug-like molecules in the SAMPL6 challenge with Drude polarizable force fields. *J. Comput.-Aided Mol. Des.* **2020**, *34*, 421−435.
(71) Pan, Z.; Huang, J.; Zhuang, W. Protein−Ligand Binding Molecular Details Revealed by Terahertz Optical Kerr Spectroscopy: A Simulation Study. *JACS Au* **2021**, *1*, 1788.
(72) Zhu, J.; Huang, J. Methylguanidinium at the Air/Water Interface: A Simulation Study with the Drude Polarizable Force Field. *J. Phys. Chem. B* **2021**, *125*, 393−405.
(73) Mendes de Oliveira, D.; Zukowski, S. R.; Palivec, V.; Henin, J.; Martinez-Seara, H.; Ben-Amotz, D.; Jungwirth, P.; Duboue-Dijon, E. Binding of divalent cations to acetate: molecular simulations guided by Raman spectroscopy. *Phys. Chem. Chem. Phys.* **2020**, *22*, 24014−24027.
(74) Zhang, P.; Han, J.; Cieplak, P.; Cheung, M. S. Determining the atomic charge of calcium ion requires the information of its coordination geometry in an EF-hand motif. *J. Chem. Phys.* **2021**, *154*, 124104.

https://doi.org/10.1021/acsphyschemau.1c00039
ACS Phys. Chem Au 2022, 2, 143−155